Bulletin of the Seismological Society of America, Vol. 96, No. 3, pp. 1114–1130, June 2006, doi: 10.1785/0120050080

Optimal Nearly Analytic Discrete Approximation to the Scalar Wave Equation

by Dinghui Yang, Jiming Peng, Ming Lu, and Tamas Terlaky

Abstract Recently, we proposed the so-called optimal nearly analytic discrete method (ONADM) for computing synthetic seismograms in acoustic and elastic wave problems (Yang *et al* 2004). In this article, we explore the theoretical properties of the ONADM including the stability criteria of the ONADM for solving 1D and 2D scalar wave equations, numerical dispersion, theoretical error, and computational efficiency when using the ONADM to model the acoustic wave fields. For comparison in the 1D case, we also discuss numerical dispersions and stability criteria of the so-called Lax–Wendroff schemes with accuracy of $O(\Delta t^4, \Delta x^8)$ and $O(\Delta t^4, \Delta x^{10})$ and the pseudospectral method (PSM). We then apply the ONADM to the heterogeneous case in synthetic seismograms. Promising numerical results illustrate that the ONADM provides a useful tool for large-scale heterogeneous practical problems because it can effectively suppress numerical dispersions caused by discretizing the wave equations when too-coarse grids are used. Numerical modeling also indicates that simultaneously using both the wave displacement and its gradients to approximate the high-order derivatives is important for decreasing the numerical dispersion and source-generated noise caused by the discretization of wave equations because wave-displacement gradients include important seismic information.

Introduction

Numerical methods for solving wave equations have provided useful tools in exploration seismology. In the forward modeling, the wave equation is typically used as an interpretive aid in complex geology or as a benchmark for testing processing algorithms. In waveform inversion for determining the earth structure, the accurate and efficient calculation of synthetic seismograms plays a key role. To solve the wave equation, we usually refer to two kinds of approximate methods. One approximate method is the perturbation method and the other is the discretization method in which we first discretize the wave equation and then solve the resulting finite-difference (FD) equations.

On the basis of finite difference approximating directly the spatial and temporal derivatives in the wave equation, many numerical methods such as the second-order center scheme (Kelly *et al.*, 1976; Zhang *et al.*, 1993, 1999; Igel *et al.*, 1995) or the high-order FD scheme (e.g., Fornberg, 1990; Igel and Weber, 1995), high-order compact schemes (Lele, 1992) (or the so-called Lax–Wendroff correction [LWC] scheme [Dablain, 1986]), and the so-called optimally accurate schemes (Geller and Takeuchi, 1998; Takeuchi and Geller, 2000) have been developed in the past two decades. Other methods also use the PSM to compute spatial derivatives (e.g., Kosloff and Baysal, 1982). In our recent works (Yang *et al.*, 2002, 2004), we have briefly discussed various theoretical properties of these algorithms.

As a perturbation method, we recently proposed a so-called optimal nearly analytic discrete method (ONADM) for acoustic and elastic equations (Yang *et al.*, 2004), which was an improved version of the nearly analytic discrete method (NADM) (Yang *et al.*, 2003a) initially suggested by Konddoh (1991) and applied to solve parabolic and hyperbolic equations (Konddoh *et al.*, 1994). The method uses a truncated Taylor expansion with respect to time to analytically approximate the wave displacement and its gradients at grid points. Meanwhile, it uses simultaneously both the wave displacement and its gradients to determine the high-order spatial derivatives involved in these truncated Taylor formulas. This is very different from other FD methods that use only the wave displacements to approximate high-order derivatives for discretizing the original wave equation. In the following sections, we will further discuss the difference between the ONADM and Lax–Wendroff/compact/optimal FD methods.

As shown by the numerical results in our earlier work (Yang *et al.*, 2004), the ONADM is very efficient in large-scale seismogram synthetics because it can effectively suppress the numerical dispersion caused by discretizing the wave equation by using the local interpolation compensation for the truncated Taylor series, whereas the conventional FD schemes with second- and fourth-order accuracies suffer

from numerical dispersion near large velocity contrast or when too few samples per wavelength are used (Fei and Larner, 1995; Yang *et al.*, 2002; Zheng *et al.*, 2006). The efficient synthetics together with algorithms for waveform inversion can help us better understand the earth structure.

The numerical tests reported in Yang *et al.* (2004) were done in a homogeneous medium. However, most seismologists employ the heterogeneous model to investigate wave propagation because the actual earth is highly heterogeneous. It is therefore necessary to examine the proposed algorithm for heterogeneous models. On the other hand, to keep numerical calculations stable and accurate, we typically require the scheme to have certain properties. The stability criterion of a numerical method is crucial in numerically synthetic seismograms because it can affect the efficiency and performance of the method. A suitable choice of space and time increments guided by the stability criteria can reduce the practical computational cost and suppress numerical dispersion, because the numerical dispersions of numerical methods are related to the so-called Courant number (Dablain, 1986; Sei and Symes, 1994), which is closely associated with the stability criteria. In this article, we investigate the stability condition of the ONADM, which can be used to further improve the computational efficiency of the algorithm.

Note that numerical dispersion has been studied as an important issue in numerical seismic simulations by many researchers. Roughly speaking, numerical dispersion is an unphysical phenomenon caused by discretizing the wave equation (Sei and Symes, 1994; Yang *et al.*, 2002). Such a phenomenon makes the wave's velocity frequency dependent. A natural idea in dealing with numerical dispersion is to use accurate methods so that dispersion errors will intrinsically be very small. For instance if one uses discrete Fourier transforms then there is no spatial numerical dispersion except for the time dispersion caused by discretizing the time derivative (Kosloff and Baysal, 1982; Fornberg, 1987). Spectral methods suffer from other drawbacks (Mizutani *et al.*, 2000), however. For example, the PSM taking the Fourier transform means that each point interacts with every other point. To some extent, this is unphysical because the interaction in dynamic elasticity is of a local nature. A remedy is to use local operators with high accuracy that are suitable for fast parallel implementation when we develop seismic models and use numerical methods to generate synthetic seismograms. Regarding the factors stated previously, the ONADM provides a useful tool for suppressing the numerical dispersion or undesirable ripples because of its nice local property as confirmed in our earlier work (Yang *et al.*, 2004). In this article, we analyze the theoretical dispersion relation of the ONADM so that we can further reduce the numerical dispersion.

The main purpose of this article is to evaluate the performance of the ONADM for general heterogeneous media and to analyze the theoretical properties of the ONADM, including the stability criteria in the 1D and 2D cases, numerical dispersion relation, computational efficiency, and theoretical error of the ONADM. For comparison, we also discuss the stability criteria and dispersion relations of the so-called LWC schemes or high-order compact schemes with eighth-order and tenth-order accuracies (Dablain, 1986) and the PSM of second-order accuracy in time (Kosloff and Baysal, 1982). Our theoretical analyses show that the numerical dispersion of the ONADM is insensitive to the Courant number as compared with the high-order compact schemes and the PSM; its Courant number limit (stability upper bound) is slightly larger than that of the PSM and slightly smaller than that of the tenth-order compact scheme in the 1D case. Meanwhile, we compare the wave-field results computed by the ONADM and the LWC methods with different accuracies in the 1D and 2D cases and the second-order central schemes in the 2D heterogeneous case.

Formulation of ONADM

The scalar wave equations in a homogeneous medium can be written as

$$\frac{\partial^2 u}{\partial t^2} = c_0^2 \frac{\partial^2 u}{\partial x^2}, \tag{1}$$

in the 1D case and

$$\frac{\partial^2 u}{\partial t^2} = c_0^2\left(\frac{\partial^2 u}{\partial x^2} + \frac{\partial^2 u}{\partial z^2}\right), \tag{2}$$

in the 2D case, where u is the wave displacement and c_0 is the sound velocity.

For computational purposes, we define the vector: $U = (u, \partial u/\partial x)^T$. Using the truncated Taylor series expansion, we obtain the following formulas:

$$U_j^{n+1} = U_j^n + \Delta t\left(\frac{\partial U}{\partial t}\right)_j^n + \frac{(\Delta t)^2}{2}\left(\frac{\partial^2 U}{\partial t^2}\right)_j^n + \frac{(\Delta t)^3}{6}\left(\frac{\partial^3 U}{\partial t^3}\right)_j^n + \frac{(\Delta t)^4}{24}\left(\frac{\partial^4 U}{\partial t^4}\right)_j^n, \tag{3}$$

and

$$U_j^{n-1} = U_j^n - \Delta t\left(\frac{\partial U}{\partial t}\right)_j^n + \frac{(\Delta t)^2}{2}\left(\frac{\partial^2 U}{\partial t^2}\right)_j^n - \frac{(\Delta t)^3}{6}\left(\frac{\partial^3 U}{\partial t^3}\right)_j^n + \frac{(\Delta t)^4}{24}\left(\frac{\partial^4 U}{\partial t^4}\right)_j^n. \tag{4}$$

Adding equations (3) and (4) together, we have

$$U_j^{n+1} = 2U_j^n - U_j^{n-1} + (\Delta t)^2\left(\frac{\partial^2 U}{\partial t^2}\right)_j^n + \frac{(\Delta t)^4}{12}\left(\frac{\partial^4 U}{\partial t^4}\right)_j^n, \tag{5}$$

where Δt is the time increment, n is the time index, and j is the space index.

The expression at the right-hand side of relation (5) is a truncated Taylor series, which only includes the even-time derivatives. To compute U_j^{n+1}, we have to calculate both $(\partial^2 U/\partial t^2)_j^n$ and $(\partial^4 U/\partial t^4)_j^n$ in formula (5). We can approximate the third and fourth terms on the right-hand side of equation (5) by the direct central difference of the derivatives $\partial^2 U/\partial t^2$ and $\partial^4 U/\partial t^4$. This would be very inefficient from a viewpoint of memory however. It is also unsatisfactory from a physically intuitive perspective because it would imply the need for additional initial conditions. A direct central difference in the time derivative would require additional grid planes and thus increase the storage requirement or lead to an implicit scheme, further resulting in higher computational complexity and more computational cost. To avoid this, we convert these high-order time derivatives to the spatial derivatives. By using such a transformation, which is similar to that used in the LWC (Lax and Wendroff, 1964; Dablain, 1986), we can rewrite equation (5) as the following:

$$U_j^{n+1} = 2U_j^n - U_j^{n-1} + (c_0\Delta t)^2 \left(\frac{\partial^2 U}{\partial x^2}\right)_j^n + \frac{(c_0\Delta t)^4}{12}\left(\frac{\partial^4 U}{\partial x^4}\right)_j^n . \quad (6)$$

Mathematically speaking, formula (6) is equivalent to the truncated Taylor expansion (5), which has lower computational accuracy regarding U_j^{n+1} because of the loss of the seismic information included in the higher-order terms in the Taylor series. According to the "analysis thought" (Konddoh, 1991; Konddoh *et al.*, 1994), we can use the interpolation function (A1) and the connection relations (A2) and (A3) (see Appendix A) to capture the lost seismic information and further increase the computational accuracy. For self-completeness, we also discuss how to evaluate the high-order spatial derivatives in formula (6) (see Appendix A).

For the 2D acoustic equation (2), we similarly have

$$\begin{aligned}\overline{U}_{i,j}^{n+1} &= 2\overline{U}_{i,j}^n - \overline{U}_{i,j}^{n-1} \\ &+ (c_0\Delta t)^2\left[\left(\frac{\partial^2 \overline{U}}{\partial x^2}\right)_{i,j}^n + \left(\frac{\partial^2 \overline{U}}{\partial z^2}\right)_{i,j}^n\right] \\ &+ \frac{(c_0\Delta t)^4}{12}\left[\left(\frac{\partial^4 \overline{U}}{\partial x^4}\right)_{i,j}^n + 2\left(\frac{\partial^4 \overline{U}}{\partial x^2\partial z^2}\right)_{i,j}^n + \left(\frac{\partial^4 \overline{U}}{\partial z^4}\right)_{i,j}^n\right],\end{aligned} \quad (7)$$

where $\overline{U}_{i,j}^n = (u, \partial u/\partial x, \partial u/\partial z)_{i,j}^T$ and (i, j) are space indices. For the high-order derivatives included in formula (7), we refer to Appendix A.

From formulas (6) and (7), we can find that the basic formulations (6) and (7) of the optimal NADM is quite similar to the LWC or compact schemes or high-order optimal FD schemes, where the original wave equation is used to convert the high-order error terms in Taylor expansions to spatial derivatives that can be handled explicitly, thereby increasing the accuracy of the method significantly (Dablain, 1986; Blanch and Robertsson, 1997; Takeuchi and Geller, 2000). The ONADM is, however, quite different from all the previously mentioned methods in the ways of approximating the higher-order spatial derivatives. From the formulations presented in Appendix A, we can see that the ONADM uses the displacement and its gradients to determine the high-order spatial derivatives, whereas the previously mentioned high-order FD methods use only the wave displacement to determine the high-order spatial derivatives and thus it is hard to capture the seismic information characterized by the gradient of wave displacement. For instance, when computing $U_{i,j}^{n+1}$ for the 2D case, the ONADM uses not only the values of the displacement u at the mesh point (i, j) and its neighboring grid points, but also the values of the partial derivatives of u with respect to spaces x and z. This allows the algorithm to capture more seismic information in both the function u^n and its gradients. Therefore, the ONADM can effectively suppress the loss of information included in the higher-order terms of the Taylor expansion, resulting in greater numerical accuracy and less numerical dispersion (Yang *et al.*, 2004). Compared with high-order FD schemes, the ONADM needs fewer grid points to achieve the same accuracy (Yang *et al.*, 2004). For example, the ONADM using three grid points in a direction has fourth-order space accuracy, the same as that of the high-order compact FD scheme (Dablain, 1986; Wang *et al.*, 2002) with five grid points. This local property that involved fewer grid points is consistent with the physical dynamic elasticity and helpful for implementation of massive parallel calculations and treatment of artificial boundaries.

Stability Criteria

It is well known that the time increment Δt must be less than or equal to the Courant limit to keep numerical calculation stable. In this section we derive the stability conditions of the ONADM for 1D and 2D cases. Our approach follows the idea by Richtmyer and Morton (1967) who presented a variety of stability analyses. Through a series of mathematical operations, we obtain the following stability condition for the 1D homogeneous case (see Appendix B):

$$\Delta t \le \alpha_{\max}\frac{h}{c_0} \approx 0.754\,\frac{h}{c_0}, \quad (8)$$

where h denotes the space increment. The maximum value $\alpha_{\max}$ (about 0.754) of Courant number defined by $\alpha = c_0\Delta t/\Delta x$ can be found in Appendix B.

For comparison and numerical dispersion analysis, we also give in Table 1 the stability conditions of the high-order LWC schemes (Dablain, 1986) for the 1D case.

From Table 1, we can see the stability condition of the ONADM is more relaxed than that of the PS method and

slightly tighter than those of the LWC methods with accuracy of $O(\Delta t^4, \Delta x^{10})$ and $O(\Delta t^4, \Delta x^8)$.

For the 2D homogeneous case, the stability condition of the ONADM (7) under the condition $\Delta x = \Delta z = h$ is given by (see Appendix B)

$$\Delta t \leq \alpha_{\max} \frac{h}{c_0} \approx 0.527 \frac{h}{c_0}. \tag{9}$$

The stability condition for a heterogeneous medium cannot be directly determined but could be approximated by using a local homogeneous method. Our conjecture is that equations (8) and (9) are approximately correct for a heterogeneous medium if the maximal value of the wave velocity c_0 is used.

Numerical Dispersion and Efficiency

In synthetic seismograms, a well-known and major artifact is the numerical dispersion limiting the usefulness of pointwise discretization schemes for the wave equation. Up to now, FD methods have been the most widely used numerical methods for wave propagation problems in seismology. Sei and Symes (1994) observed that the higher the order of the FD schemes, the less dispersion is experienced by the wave. This motivates us to use high-order FD schemes (e.g., tenth-order method; Dablain, 1986) to reduce the numerical dispersion. A higher-order FD method requires more floating point operations, however, because, in general, it involves more grid points in a direction. The demand of more grids in higher-order FD methods prevents the algorithms from efficient parallel implementation and artificial boundary treatment. Another way of attacking the numerical dispersions is to use the so-called flux-corrected transport (FCT) technique, which typically is unable to fully recover the lost resolution by the numerical dispersion when the spatial sampling becomes too coarse (Yang *et al.*, 2002). In this section, following the analysis methods of the cited references (Vichnevetsky, 1979; Dablain, 1986; Wang *et al.*, 2002) we investigate the dispersion relation of the ONADM for the 1D case so that we can further reduce the numerical dispersion depending on the Courant number of the method. For comparison, we also present the dispersion relations of the LWC or high-order compact schemes with eighth- and tenth-order accuracy and the PS method.

In the following, we show the numerical results using the dispersion relations (C3) and (C5). The detailed analyses of the dispersion relations of the ONADM and the so-called LWC with different orders (Dablain, 1986) are presented in Appendix C.

Figures 1–4 plot the dispersion relations for the ONADM, spectral method (Kosloff and Baysal, 1982), and the high-order LWC with accuracies of $O(\Delta t^4, \Delta x^8)$ and $O(\Delta t^4, \Delta x^{10})$ for the 1D homogeneous wave equation corresponding to different Courant numbers. We point out that all the experiments in this work are done on a Pentium 4 PC with 256 MB RAM.

Figure 1 shows that the numerical velocity of the ONADM gradually approximates the exact wave velocity whereas the Courant number α increases in the high-

Table 1
The Approximate Maximum Courant Numbers of Different Methods for the 1-D Case

Methods	ONADM	PSM	$O(\Delta t^4, \Delta x^{10})$ LWC	$O(\Delta t^4, \Delta x^8)$ LWC
$\alpha_{\max}$	0.754	0.6366	0.893	0.929

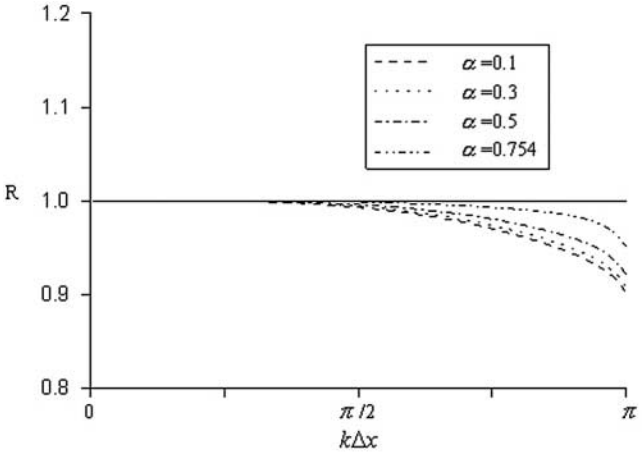

Figure 1. The ratio R_{ONADM} (formula C3) of the numerical velocity to the phase velocity versus wavenumber $k\Delta x$ for the ONADM for different Courant numbers $\alpha = c_0\Delta t/\Delta x$, where four lines correspond to $\alpha = 0.1$, 0.3, 0.5, and $\alpha_{\max}$, respectively.

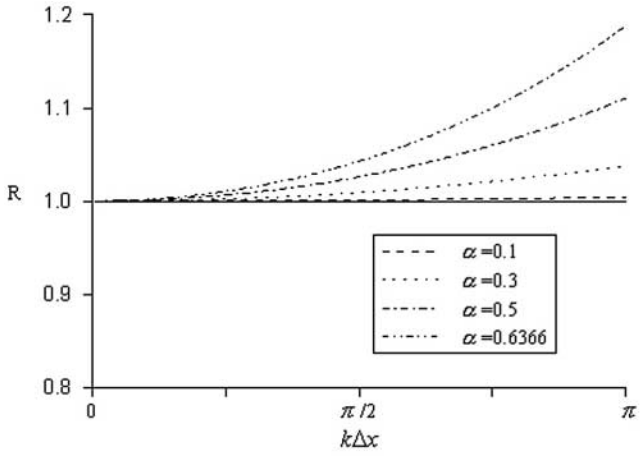

Figure 2. The ratio of the numerical velocity to the phase velocity versus wavenumber $k\Delta x$ for the pseudospectral method (Kosoff and Baysal, 1982) for different Courant numbers $\alpha = c_0\Delta t/\Delta x$, where four lines correspond to $\alpha = 0.1$, 0.3, 0.5, and $\alpha_{\max}$, respectively.

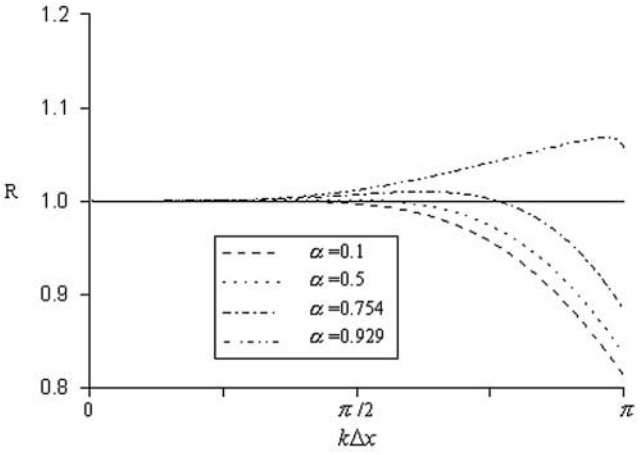

Figure 3. The ratio $R_{\text{L-W}}$ (formula C5) of the numerical velocity to the phase velocity versus wavenumber $k\Delta x$ for the eighth-order LWC (Dablain, 1986) for different Courant numbers $\alpha = c_0\Delta t/\Delta x$, where four lines correspond to $\alpha = 0.1$, 0.5, 0.754, and $\alpha_{\max}$, respectively.

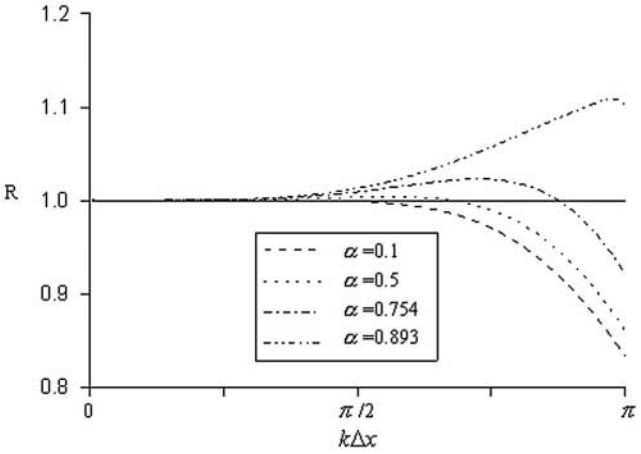

Figure 4. The ratio $R_{\text{L-W}}$ (formula C5) of the numerical velocity to the phase velocity versus wavenumber $k\Delta x$ for the tenth-order LWC (Dablain, 1986) for different Courant numbers $\alpha = c_0\Delta t/\Delta x$, where four lines correspond to $\alpha = 0.1$, 0.5, 0.754, and $\alpha_{\max}$, respectively.

frequency range. It also shows that at the stability limit ($\alpha = c_0\,\Delta t/\Delta x \approx 0.754$), the numerical dispersion is minimal. This suggests that we can minimize the numerical dispersion caused by the ONADM by using the maximum Courant number and the PSM will have the maximal dispersion error (Fig. 2) in a similar scenario. Moreover, the change of numerical dispersion corresponding to the change of the Courant number α is not sensitive as compared with the spectral method (Fig. 2) and the high-order LWC with accuracies of $O(\Delta t^4, \Delta x^8)$ and $O(\Delta t^4, \Delta x^{10})$ (Fig. 3 and 4). This property is useful in practical calculations because we do not need to consider how to choose appropriate Courant numbers in the stability range. From Figure 2 we observe that the numerical velocity for the PSM (Kosloff and Baysal, 1982) is usually greater than the exact velocity. This shows that the dispersion in the PSM leads the exact signal whereas the dispersion in the ONADM follows the signal. However, as we observed in Figures 3 and 4, even for a fixed Courant number, the dispersion of the high-order LWC is irregular. It sometimes leads the exact signal and sometimes follows the signal. This phenomenon indicates that it is hard to choose a suitable Courant number for the high-order LWC.

Next we investigate the numerical dispersion and computational efficiency of the 2D ONADM through modeling waveforms. For this case under our present consideration, the wave equation in a homogeneous medium is described by

$$\frac{\partial^2 u}{\partial t^2} = c_0^2\left(\frac{\partial^2 u}{\partial x^2} + \frac{\partial^2 u}{\partial z^2}\right) + f, \tag{10}$$

where the wave velocity is defined by $c_0 = \sqrt{\mu/\rho}$, in which μ and ρ are the elastic constant and density of the medium, and f is the force source. In this numerical experiment, we choose $\mu = 6.25$ GPa and $\rho = 2.1$ g/cm^3. We choose the Courant number $\alpha = c_0\Delta t/\Delta x \approx 0.1035$ and the computational domain is $0 \le x \le 9.95$ km, $0 \le z \le 9.95$ km. The source is an explosive source that is located at the center of the computational domain and has a Ricker wavelet with a peak frequency of $f_0 = 15$ Hz. The time variation of the source function is $\sin(2\pi f_0 t)\exp(-4\pi^2 f_0^2 t^2/16)$ (Zahradnik *et al.*, 1993).

Figure 5 shows the wave-field snapshots at $t = 1.6$ sec on a coarse grid ($\Delta x = \Delta z = 50$ m), generated respectively by the fourth-order LWC, the eighth-order LWC (Dablain, 1986), and the ONADM, whereas Figure 6 shows the wave-field snapshots at $t = 1.6$ sec under the same Courant number α and on a fine grid, generated by the fourth-order LWC ($\Delta x = \Delta z = 10$ m) and eighth-order LWC ($\Delta x = \Delta z = 15$ m) methods. We can see that the wavefronts of seismic waves shown in Figure 5, simulated by the so-called LWC (Dablain, 1986) and the ONADM, are identical. However, the wave-field snapshot (Fig. 5c), generated by the ONADM, shows that the ONADM has much less numerical dispersion even if the space increment chosen is 50 m without any additional treatments, whereas the LWC with accuracies of $O(\Delta t^4, \Delta x^4)$ and $O(\Delta t^4, \Delta x^8)$ suffer from serious numerical dispersions (see Fig. 5a and b). Comparison between Figure 5c and Figure 6 demonstrates that the ONADM can provide the same accuracy as those of the so-called LWC with accuracies of $O(\Delta t^4, \Delta x^4)$ and $O(\Delta t^4, \Delta x^8)$ on a fine grid under the same Courant number. But the computational cost of the ONADM is quite different from those of the LWC methods. For example, it took the ONADM about 1.86 min to generate Figure 5c, whereas the LWC method took about 108 and 38.7 min to generate Fig. 6a and b, respectively. This suggests that the computational speed of the ONADM is roughly 21

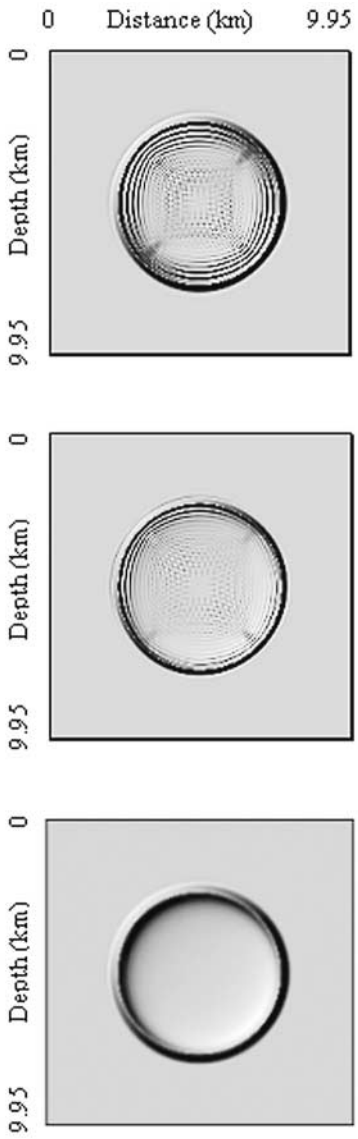

Figure 5. Snapshots of seismic wave fields at time 1.6 sec on the coarse grid ($\Delta x = \Delta z = 50$ m), generated by the fourth-order LWC method (a), the eighth-order LWC method (b), and the ONADM (c).

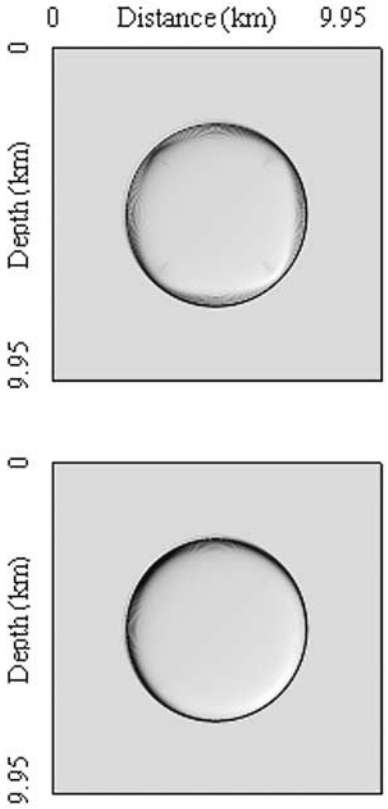

Figure 6. Snapshots of seismic wave fields at time 1.6 sec on the fine grid, generated by the fourth-order LWC method ($\Delta x = \Delta z = 10$ m) (a) and the eighth-order LWC method ($\Delta x = \Delta z = 15$ m) (b).

times the eighth-order LWC and about 58 times of the fourth-order LWC on a fine grid to achieve the same accuracy as that of the ONADM. Note that the computational cost of the ONADM is more expensive than the higher-order LWC on the same coarse grid. Meanwhile, the storage space required for computation in the ONADM is also different from those of the LWC methods. The ONADM needs nine arrays to store wave displacement $u_{i,j}^{n+1}$, $u_{i,j}^{n}$, $u_{i,j}^{n-1}$, and its gradients at each spatial grid point, and the number of grid points is 200×200 on a coarse grid for generating Figure 5c. The high-order LWC needs only these arrays to store the wave displacement at each grid point, but the number of grid points on a fine grid for generating Figure 6a and b goes up to 996×996 for the fourth-order LWC and 664×664 for the eighth-order LWC, respectively. It indicates that the ONADM requires only roughly 12% of storage space of the fourth-order LWC and about 27% of storage space of the eighth-order LWC.

Error Analysis

In our earlier work (Yang *et al.*, 2004), we discussed the numerical error of the ONADM and compared the numerical solutions of the ONADM with the analytical solution of the 2D acoustic wave equation (2). In this article we analyze the theoretical error for the scalar wave problem via the Taylor series expansion. For the 1D case, we have the following theoretical error of the ONADM from equations (D7) and (D9) presented in Appendix D:

$$\begin{aligned} E &= [(D_{2t} - L_{2t}) - (D_{2x} - c_0^2 L_{2x})]U_j^n \\ &= -c_0^2\left[\frac{(\alpha^4 + 1)\Delta x^4}{360}\left(\frac{\partial^6 u}{\partial x^6}\right)_j^n, \frac{(7\alpha^4 + 3)\Delta x^4}{2520}\left(\frac{\partial^7 u}{\partial x^7}\right)_j^n\right]^T \\ &\quad + O(\Delta x^6 + \Delta t^6) = O(\Delta x^4 + \Delta t^6), \end{aligned} \tag{11}$$

where D_{2t}, L_{2t}, D_{2x}, and L_{2x} are the exact derivative and the

ONADM difference operators with respect to time and space, respectively, whose definitions are given in Appendix D.

For the 2D case, we have the following theoretical error E, derived from equations (D10), (D13), and (D14) as discussed in the Appendix D:

$$E = O(\Delta t^6 + \Delta x^4) . \tag{12}$$

From error (11), we can see that the error of the ONADM is related to the Courant number α. To demonstrate the effect of the Courant number α on the error of the ONADM, we consider the following 1D initial problem:

$$\frac{\partial^2 u}{\partial t^2} = c_0^2 \frac{\partial^2 u}{\partial x^2}, \tag{13a}$$

$$u(0,x) = \cos\left(-\frac{2\pi f_0}{c_0} \cdot x\right), \quad \text{and} \tag{13b}$$

$$\frac{\partial u(0,x)}{\partial t} = -2\pi f_0 \cdot \sin\left(-\frac{2\pi f_0}{c_0} \cdot x\right), \tag{13c}$$

where f_0 is the frequency and c_0 is the wave velocity.

In the numerical example, we choose the number of grid points $N = 200$, the frequency $f_0 = 15$ Hz, and the wave velocity $c_0 = 6000$ m/sec. The relative error (E_r) is the ratio of the root-mean-square (rms) of the residual ($u_i^n - u(t_n, x_i)$) and the rms of the exact solution $u(t_n, x_i)$. Its explicit definition is as follows:

$$E_r(\%) = \left\{ \frac{1}{\sum_{i=1}^{N} [u(t_n, x_i)]^2} \sum_{i=1}^{N} [u_i^n - u(t_n, x_i)]^2 \right\}^{1/2} \times 100. \tag{14}$$

Figure 7 shows the computational results of the relative error E_r at different times, where three lines of E_r corresponding to the Courant numbers of $\alpha = 0.2$, 0.5, and 0.75 are shown in a semilog scale. Figure 8 plots the relative errors E_r versus Courant numbers at different calculation time $t = 1.8$ sec, 1.2 sec, and 0.6 sec. From Figures 7 and 8, we can conclude that the error introduced by the ONADM measured by E_r tends to decrease as the Courant number increases. It suggests that we can reduce the numerical errors through choosing the maximum Courant number.

Numerical Modeling

In this section, we test the ONADM for 2D heterogeneous isotropic media. To start, we first compare the synthetic seismograms for the 1D case, computed by the ONADM and the LWC with accuracies of $O(\Delta t^4, \Delta x^{10})$ and $O(\Delta t^4, \Delta x^4)$ (Dablain, 1986).

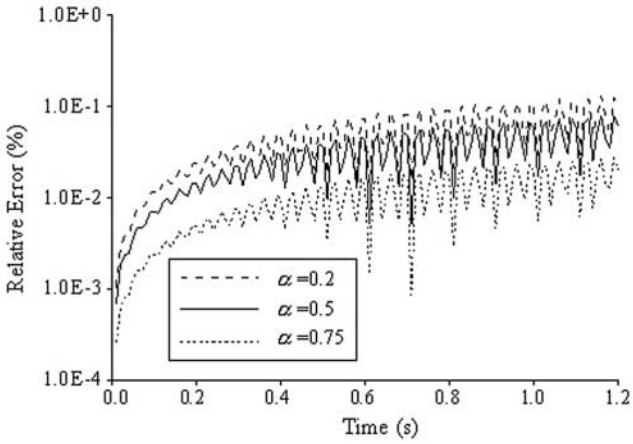

Figure 7. The relative errors of the ONADM measured by E_r are shown in a semilog scale for the 1D initial problem (13), where three lines correspond to different Courant numbers $\alpha = 0.2$, 0.5, and 0.75, respectively.

1D Case

The velocity model is selected for our comparative study, as illustrated in Figure 9 (similar to the model of Dablain [1986]). The distance from the source to the farthest receiver is 5.28 km. The total model domain is 10.4 km long. The source is an explosive source that is at coordinate $z_s = 2.6$ km and has a Ricker wavelet with a peak frequency of $f_0 = 20$ Hz. The time variation of the source function is $\sin(2\pi f_0 t) \exp(-4\pi^2 f_0^2 t^2/16)$. The receiver positions are located at $z_s = 3.9$, 6.5, and 7.8 km, respectively. Other parameters are chosen as the minimum velocity, 2500 m/sec; the maximum velocity, 3700 m/sec; the spatial increment, $\Delta x = 10$ m; and the time increment $\Delta t = 0.002$ sec resulting in the maximum Courant number $\bar{\alpha}_{\max} = c_{\max}\Delta t/\Delta x = 0.74$. Total data length is 2.4 sec.

Figures 10, 11, and 12 show the primary arrivals at receivers 1, 2, and 3, computed by the ONADM, the $O(\Delta t^4, \Delta x^{10})$ and $O(\Delta t^4, \Delta x^4)$ LWC methods, respectively. Figures 10 and 11 show that the waveforms generated by the ONADM are identical with those computed by the $O(\Delta t^4, \Delta x^{10})$ LWC except for marginal difference near wave peaks, whereas the $O(\Delta t^4, \Delta x^4)$ LWC scheme suffers from seriously numerical dispersions (see Fig. 12). This verifies the convergence of the ONADM because the convergence of the $O(\Delta t^4, \Delta x^{10})$ LWC was demonstrated and equivalent with the PSM in Dablain's study (Dablain, 1986). In Figure 11, we can also see the anomalous dispersion leading the exact signal, which is the same as that exhibited by the PSM (Dablain, 1986).

2D Heterogeneous Case

To demonstrate the performance of the ONADM in the 2D heterogeneous case, we choose three models for testing. In our experiments, the 2D heterogeneous wave equation is:

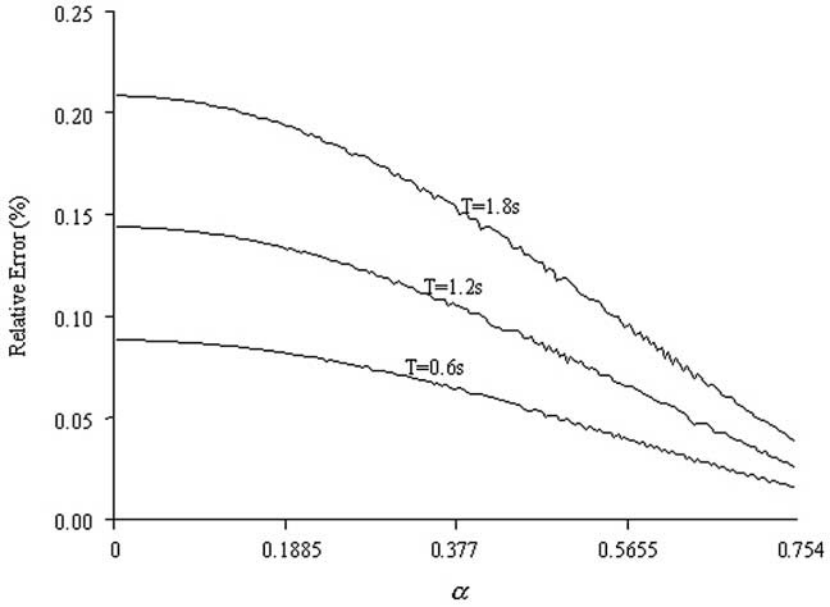

Figure 8. The relative errors of the NADM versus Courant number α, measured by E_r, are shown in a semilog scale for the 1D initial problem (13), where three lines correspond to different times $T = 0.6$ sec, 1.2 sec, and 1.8 sec, respectively.

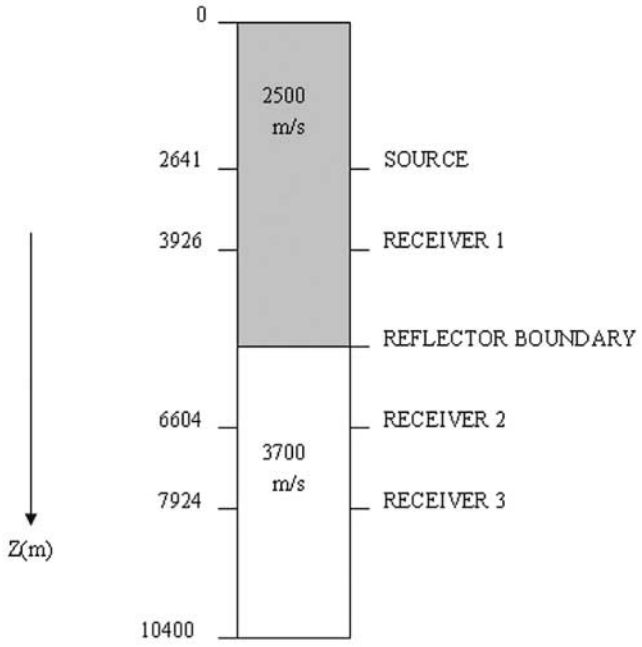

Figure 9. One-dimensional model for comparisons between the ONADM and the high-order LWC methods.

$$\frac{\partial^2 u}{\partial t^2} = \frac{1}{\rho(x,z)}\left[\frac{\partial}{\partial x}\left(\mu(x,z)\,\frac{\partial u}{\partial x}\right) + \frac{\partial}{\partial z}\left(\mu(x,z)\,\frac{\partial u}{\partial z}\right)\right] + \frac{f}{\rho(x,z)}, \quad (15)$$

where $\rho(x,z)$ is the density, $\mu(x,z)$ is the elastic parameter, f is the source function with the same time variation function as that of the 1D case in the following numerical experiments.

Model 1. In our first example, we choose the model of two-layer media with the curve inner interface governed by the following depth function:

$$z = 1 + \frac{1}{2}\left(1 + \sin\frac{2\pi(7.5 - x)}{10}\right), \quad 0 \le x \le 10 \text{ km}.$$

The medium model was shown in Figure 13, where the medium parameters are chosen by: $\mu_1(x,z) = 25.4$ GPa, $\rho_1(x,z) = 1.8$ g/cm^3, $\mu_2(x,z) = 26.672$ GPa, $\rho_2(x,z) = 3.0$ g/cm^3, corresponding to the top (subscript 1) and bottom (subscript 2) layers, respectively. The computational domain is $0 \le x \le 10$ km, $0 \le z \le 3$ km. We choose the spatial increment $\Delta x = \Delta z = 20$ m, the time increment $\Delta t = 2 \times 10^{-3}$ sec, and the number of grid points 501×151. The source is an explosive source that is at coordinate $(x_s, z_s) = (5$ km, 0.06 km) and has a Ricker wavelet with a peak frequency of $f_0 = 15$ Hz. The wave fields are recorded by 501 receivers on the surface spread from $x = 0$ to $x = 10$ km spaced 0.02 km apart.

Figures 14 and 15 are the synthetic seismograms generated by the ONADM. In Figure 14 the reflected waves from the curve inner interface and the free surface are very clear. We can identify clearly the structure of medium from the reflected curve wave shown in Figure 14 for the chosen medium model. But when we choose the density $\rho_2(x,z) = 2.0$ g/cm^3 and keep other parameters the same as in the synthetic seismogram shown in Figure 14, because the wave impedance under this case is smaller than that used in Figure 14, we cannot see the reflected curve wave from Figure 15. To generate the synthetic seismograms (Figs. 14 and 15), the

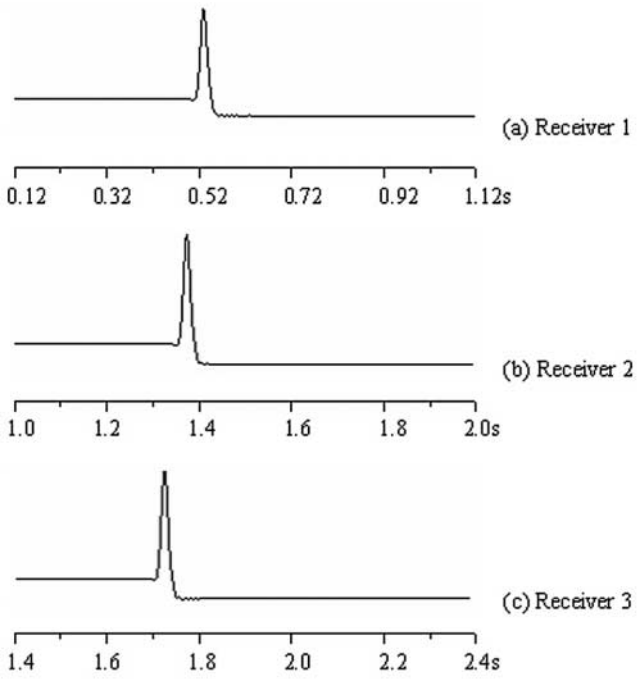

Figure 10. The waveforms generated by the ONADM for the 1D case.

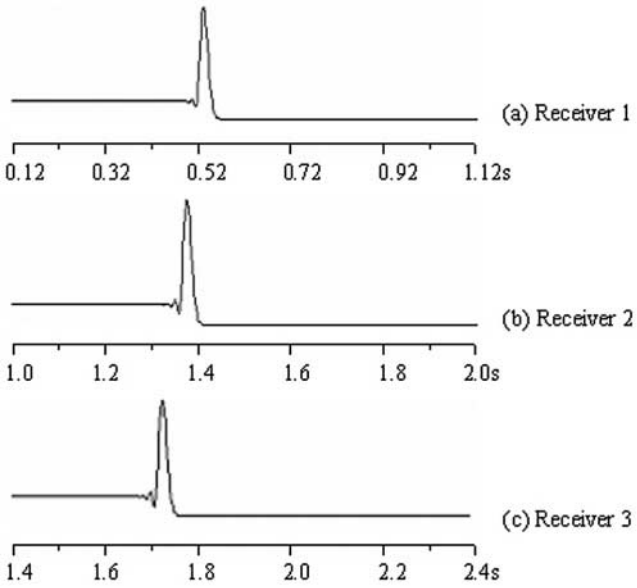

Figure 11. The waveforms generated by the $O(\Delta t^4, \Delta x^{10})$ LWC method (Dablain, 1986) for the 1D case.

ONADM took about 6 min for model 1. In this experiment, we use the four-times absorbing boundary condition developed by Higdon (1991) and discretized by Yang *et al.* (2003b) based on the stable biased center scheme.

Model 2. In this experiment, we compare the performances of the ONADM and the second-order FD method for the complete heterogeneous problem. We consider a two-layer heterogeneous medium whose density and elastic parameters are as follows:

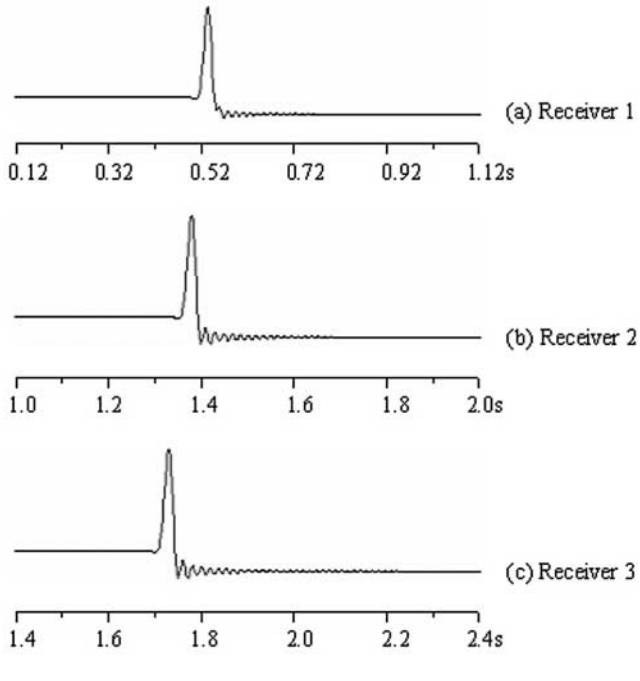

Figure 12. The waveforms generated by the $O(\Delta t^4, \Delta x^4)$ LWC method (Dablain, 1986) for the 1D case.

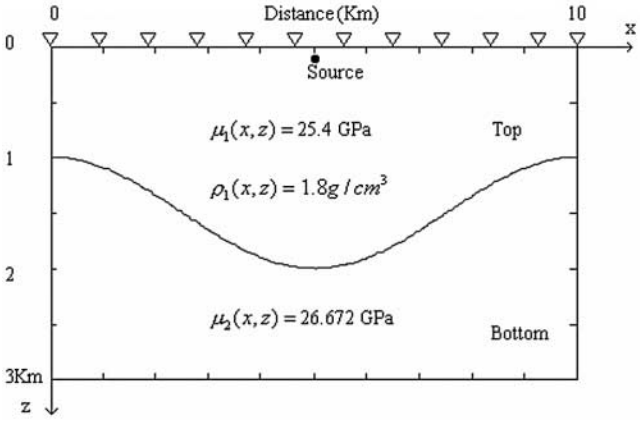

Figure 13. Two-dimensional medium model with an inner-curve interface.

$$\rho(x,z) = \rho_0 * \left(1 + \frac{x}{50}\right),$$

$$\mu(x,z) = 16 + \frac{x}{4} + \frac{z}{2},$$

where the constant density ρ_0 equals 2.1 g/cm^3 and 3.0 g/cm^3 for the upper and bottom layers, respectively. The horizontal inner interface is located at the depth $z = 3.924$ km.

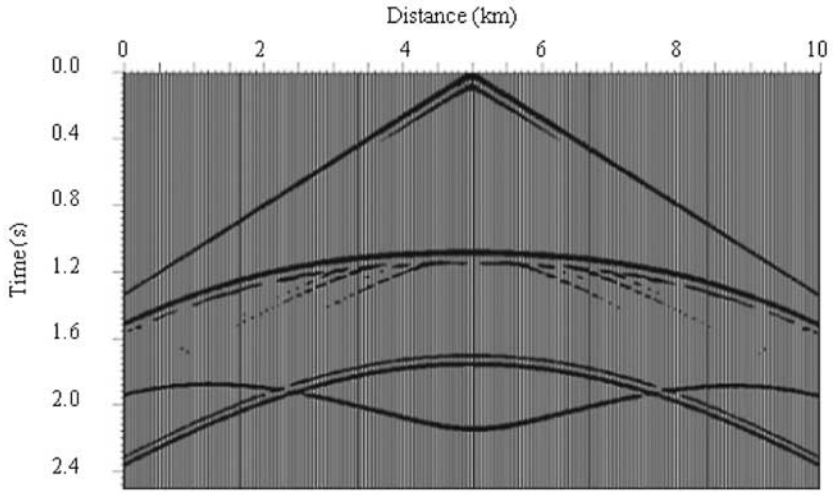

Figure 14. The synthetic seismogram on the surface, generated by the ONADM for the 2D model 1 with $\rho_2(x, z) = 3.0$ g/cm^3 shown in Figure 13.

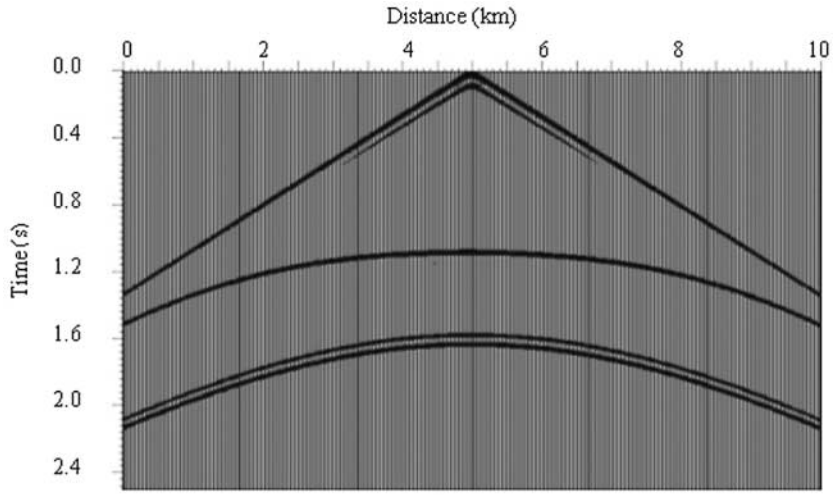

Figure 15. The synthetic seismogram on the surface, generated by the ONADM for the 2D model 1 with $\rho_2(x, z) = 2.0$ g/cm^3 shown in Figure 13.

In the example, the computational domain is chosen as $0 \le x \le 6.048$ km, $0 \le z \le 6.048$ km. The source is an explosive source that is at coordinate $(x_s, z_s) = (3.024$ km, 3.024 km) and has a Ricker wavelet with a peak frequency of $f_0 = 15$ Hz. The time variation of the source is the same as that in the 1D case. Three receivers are at $(x_1, z_1) = (4.464$ km, 1.404 km), $(x_2, z_2) = (4.464$ km, 1.764 km), and $(x_3, z_3) = (4.464$ km, 2.124 km).

The waveforms, generated by the ONADM and the second-order central FD method (Kelly *et al.*, 1976), are compared in Figures 16 and 17. The coarse spatial step in the ONADM computations is chosen by $\Delta x = \Delta z = 36$ m. The time increment is $\Delta t = 4.6 \times 10^{-3}$ sec. To generate Figure 17, the fine-grid step is chosen by $\Delta x = \Delta z = 6$ m, the time increment is chosen by $\Delta t = 1.15 \times 10^{-3}$ sec, resulting in a Courant number that is about 1.5 times of that used in the ONADM calculation. Figures 16 and 17 show that the waveforms generated by the ONADM on the coarse grids are identical with those computed by the second-order FD method on the fine grids except for a slight difference behind the main wave peak. The difference is mainly caused by the numerical dispersions and the source-generated noises (artifacts due to source location at grid points). But from Figure 16 we can observe that the ONADM has fairly less numerical dispersions when the coarse-grid step is used. It indicates that the ONADM enables wave propagation to be simulated in large-scale heterogeneous models through using coarse grids. This is the main reason that leads to the great efficiency of the ONADM. For example, in our experiments, it took the ONADM about 45 sec central processing unit (CPU) time to generate Figure 16, whereas generating Figure 17 in the same computer environments costs the second-order FD about 14 min. The required storage for the FD method is about 12 times of that for the ONADM.

Model 3. To further investigate the performance of the ONADM for the large heterogeneous model, we choose the computational domain as $0 \le x \le 16$ km, $0 \le z \le 16$ km, and the number of grid points 401×401. The source is located at the center of the computational domain and the horizontal inner interface is at $z = 9.4$ km. The spatial and time increments are $\Delta x = \Delta z = 40$ m and $\Delta t = 6.7 \times$

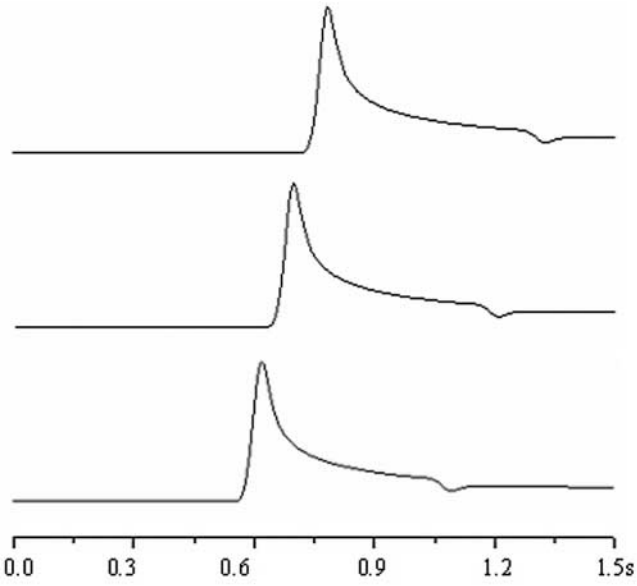

Figure 16. The waveforms generated by the ONADM on the coarse grid ($\Delta x = \Delta z = 36$ m) for the 2D heterogeneous model 2.

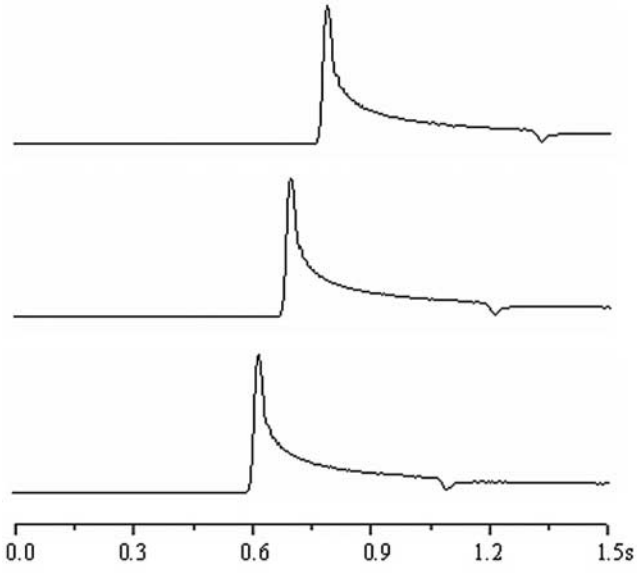

Figure 17. The waveforms generated by the second-order FD method (Kelly *et al.*, 1976) on the fine grid ($\Delta x = \Delta z = 6$ m) for the 2D heterogeneous model 2.

10^{-3} sec so that the maximum value of the Courant number α is about 0.526. The remaining parameters are the same as those used in model 2.

Figure 18 is the wave-field snapshot at $t = 2.5$ sec generated by the ONADM. From the wave-field snapshot, we can clearly observe the reflection of the acoustic wave from the inner interface, and the computation is stable for the Courant number 0.526 that approaches the maximum Courant number of keeping the ONADM stable. The wave-field snapshot also shows that the ONADM has less numerical dispersions even if the space increment chosen is 40 m without any additional treatments. It took the ONADM about 7 min to finish the job.

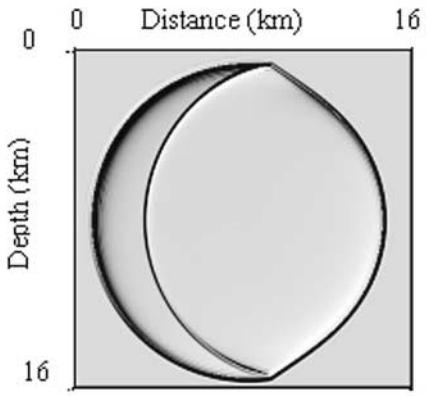

Figure 18. Snapshot of the seismic wave field at time 2.5 sec in a heterogeneous two-layer isotropic medium, generated by the ONADM.

Discussion and Conclusions

In this article, we have discussed the difference among the ONADM, the Lax–Wendroff/compact, and optimal FD methods. Our theoretical analysis shows that the ONADM has fourth-order accuracy in space and sixth-order accuracy in time. The stability conditions of the ONADM for 1D and 2D cases when it is applied to the scalar wave equation are also explored. Numerical simulations with large Courant numbers for 1D and 2D problems demonstrate the efficiency of the stability conditions obtained in our present study. Numerical dispersion analysis shows that we can minimize the numerical dispersion through using the optimal Courant number that approximately equals the maximum Courant number $\alpha_{\max}$ for the ONADM. The grid dispersion of the ONADM lessens with increasing the Courant number α, and the numerical dispersion reaches its minimum when the Courant number α equals the stability limit $\alpha_{\max} \approx 0.754$ for the 1D case. Generally speaking, the grid dispersion of the ONADM is smaller than those of the high-order compact or so-called LWC with accuracies of $O(\Delta t^4, \Delta x^8)$ and $O(\Delta t^4, \Delta x^{10})$ (Dablain, 1986) in the high-frequency range; the maximum numerical error of the ONADM decreases as the Courant number increases. In other words, when the frequency and spatial increment are constants, through increasing the time increment without violating the stability conditions (8) for the 1D case and (9) for the 2D case, we can not only lessen simultaneously the numerical dispersion (see Fig. 1) and numerical errors (see Figs. 7 and 8), but also reduce computational cost.

From comparing the wave-field snapshots (Fig. 5) and acoustic seismograms shown in Figures 10, 11, 12, and the

dispersion curves presented in this article, we can conclude that the relation between numerical dispersion caused by the discretization of wave equations and the accuracy of numerical methods is not directly proportional though decreasing the numerical dispersion with increasing the accuracy of numerical methods. In other words, increasing the accuracy of methods does not result in a proportional decrease of the numerical dispersion. This conclusion can also be verified from both numerical dispersion curves and wave-field snapshots computed by using various accurate FD schemes presented in Wang *et al.* (2002). Numerical results also illustrate that simultaneously using both the wave displacement and its gradients to approximate the high-order derivatives is important for decreasing the numerical dispersion and source-generated noises (artifacts due to source location at grid points) caused by discretizing wave equations because displacement gradients include important seismic information. Numerical modeling also indicates that the gradient of wave displacement is an important control of decreasing the grid dispersion. It suggests that we should consider the wave-gradient field when we design a new numerical method to solve the acoustic wave equation.

The introduction of the local connection relations (A2) and (A3) greatly improves the continuity and derivability of the approximate function U^n (because U^n is an approximate variable during data processing). The local connection relation (A3) of the displacement gradient also improves the continuity of the stress at the inner interface. From the examples presented in Figures 14, 15, 16, and 18, we see that the ONADM can capture effectively the inner interface without any special treatments at the discontinuity; therefore, it can simulate seismic waves in complex geometries and heterogeneous media without any additional treatments.

It is true that the CPU time of the ONADM in per iteration is more than that of the high-order LWC. For example, the overall computational cost of the ONADM is about 2.5 times of the eighth-order LWC and about 2.1 times of fourth-order LWC because of the added gradient computation in the ONADM. However, because the ONADM yields less numerical dispersion than the LWC with the accuracy of fourth and eighth orders, we can reduce the computational cost through adopting coarser spatial increments to achieve the same accuracy as that of the LWC on a finer grid with smaller timesteps. Consequently, the overall computational speed of the ONADM is much faster than that of the higher-order LWC. This was confirmed by our numerical experiments as discussed in the section of numerical dispersion.

This study also indicates that the ONADM can be directly applied to the heterogeneous case without any additional treatments because the gradients of the wave displacement are simultaneously computed in the ONADM, whereas the so-called LWC schemes (Dablain, 1986) can be not directly applied the heterogeneous problem because equation (15) may involve the displacement gradients. Synthetic seismograms generated by the ONADM for the heterogeneous problem illustrate that the ONADM can effectively suppress numerical dispersions and source noises when too-coarse computation grids are used. This further demonstrates that the ONADM enables wave propagation in heterogeneous media to be simulated in large-scale models through using the coarse computation grids.

Acknowledgments

We thank Dr. Fred F. Pollitz (associate editor) and the anonymous reviewer for their valuable comments that substantially improved the presentation of the article. This work was supported by the National Natural Sciences Foundation of China (Grant 40574014), the MCME of China, and the MITACS project "New interior point methods and software for convex conic linear optimization with applications to solving VLSI circuit layout problems." The research of J.P. was supported in part by the Grant RPG 249635-02 of the National Sciences and Engineering Research Council of Canada (NSERC), a PREA award from Ontario, and the MITACS project.

References

Blanch, J. O., and J. O. A. Robertsson (1997). A modified Lax-Wendroff correction for wave propagation in media described by Zener elements, *Geophys. J. Int.* **131,** 381–386.

Dablain, M. A. (1986). The application of high-order differencing to the scalar wave equation, *Geophysics* **51,** 54–66.

Fei, T., and K. Larner (1995). Elimination of numerical dispersion in finite-difference modeling and migration by flux-corrected transport, *Geophysics* **60,** 1830–1842.

Fornberg, B. (1987). The pseudospectral method: comparisons with finite difference for the elastic wave equation, *Geophysics* **52,** 483–501.

Fornberg, B. (1990). High-order finite differences and pseudo-spectral method on staggered grids, *SIAM J. Numer. Anal.* **27,** 904–918.

Geller, R. J., and N. Takeuchi (1998). Optimally accurate second-order time-domain finite difference scheme for the elastic equation of motion: one-dimensional case, *Geophys. J. Int.* **135,** 48–62.

Higdon, R. L. (1991). Absorbing boundary conditions for elastic waves, *Geophysics* **56,** 231–241.

Igel, H., and M. Weber (1995). SH-wave propagation in the whole mantle using high-order finite differences, *Geophys. Res. Lett.* **22,** 731–734.

Igel, H., P. Mora, and B. Riollet (1995). Anisotropic wave propagation through finite-difference grids, *Geophysics* **60,** 1203–1216.

Kelly, K., R. Ward, S. Treitel, and R. Alford (1976). Synthetic seismograms: a finite-difference approach, *Geophysics* **41,** 2–27.

Konddoh, Y. (1991). On thoughts analysis of numerical scheme for simulation using a Kernel Optimum Nearly-Analytical Discretization (KOND) method, *J. Phys. Soc. Jpn.* **60,** 2851–2861.

Konddoh, Y., Y. Hosaka, and K. Ishii (1994). Kernel optimum nearly-analytical discretization algorithm applied to parabolic and hyperbolic equations, *Comput. Math. Appl.* **27,** 59–90.

Kosloff, D., and E. Baysal (1982). Forward modeling by a Fourier method, *Geophysics* **47,** 1402–1412.

Lax, P. D., and B. Wendroff (1964). Difference schemes for hyperbolic equations with high order of accuracy, *Commun. Pure Appl. Math.* **17,** 381–398.

Lele, S. K. (1992). Compact finite difference schemes with spectral-like resolution, *J. Comput. Phys.* **103,** 16–42.

Mizutani, H., R. J. Geller, and N. Takeuchi (2000). Comparison of accuracy and efficiency of time-domain schemes for calculating synthetic seismograms, *Phys. Earth Planet. Interiors* **119,** 75–97.

Richtmyer, R. D., and K. W. Morton (1967). *Difference Methods for Initial Value Problems*, Interscience, New York.

Sei, A., and W. Symes (1994). Dispersion analysis of numerical wave propagation and its computational consequences, *J. Sci. Comput.* **10,** 1–27.

Takeuchi, N., and R. J. Geller (2000). Optimally accurate second order time-domain finite difference scheme for computing synthetic seismograms in 2-D and 3-D media, *Phys. Earth Planet. Interiors* **119,** 99–131.

Wang, S. Q., D. H. Yang, and K. D. Yang (2002). Compact finite difference scheme for elastic equations, *J. Tsinghua Univ. Sci. Tech.* **42,** 1128–1131 (in Chinese).

Vichnevetsky, R. (1979). Stability charts in the numerical approximation of partial differential equations: a review, *Math. Comput. Simul.* **21,** 170–177.

Yang, D. H., E. Liu, Z. J. Zhang, and J. Teng (2002). Finite-difference modelling in two-dimensional anisotropic media using a flux-corrected transport technique, *Geophys. J. Int.* **148,** 320–328.

Yang, D. H., M. Lu, R. S. Wu, and J. M. Peng (2004). An optimal nearly analytic discrete method for 2D acoustic and elastic wave equations, *Bull. Seism. Soc. Am.* **94,** 1982–1992.

Yang, D. H., J. W. Teng, Z. J. Zhang, and E. Liu (2003a). A nearly-analytic discrete method for acoustic and elastic wave equations in anisotropic media, *Bull. Seism. Soc. Am.* **93,** 882–890.

Yang, D. H., S. Q. Wang, Z. J. Zhang, and J. W. Teng (2003b). n-times absorbing boundary conditions for compact finite difference modeling of acoustic and elastic wave propagation in the 2-D TI Medium, *Bull. Seism. Soc. Am.* **93,** 2389–2401.

Zahradnik, J., P. Moczo, and T. Hron (1993). Testing four elastic finite-difference schemes for behavior at discontinuities, *Bull. Seism. Soc. Am.* **83,** 107–129.

Zhang, Z. J., Q. D. He, and J. W. Teng (1993). Simulation of 3-component seismic records in a 2-dimensional transversely isotropic media with finite diffence method, *Can. J. Expl. Geophys.* **29,** 51–58.

Zhang, Z. J., G. J. Wang, and J. M. Harris (1999). Multi-component wavefield simulation in viscous extensively dilatancy anisotropic media, *Phys. Earth Planet. Interiors* **114,** 25–38.

Zheng, H. S., Z. J. Zhang, and E. Liu (2006). Nonlinear seismic wave propagation in anisotropic media using the flux-corrected transport technique, *Geophys. J. Int.* (in press).

Appendix A

Evaluation of High-Order Derivatives

To apply formula (6) to compute the values of U at time t_{n+1} in synthetic seismograms, we need the high-order derivatives including equation (6). To determine the high-order derivatives, following the "analysis thought" (Konddoh *et al.*, 1994), we use the following interpolation function of the spatial step Δx:

$$G(\Delta x) = \sum_{r=1}^{5} \frac{1}{r!} \left(\Delta x \frac{\partial}{\partial x} \right)^r u, \tag{A1}$$

and construct the following connection relations:

$$[G(-\Delta x)]_j^n = u_{j-1}^n, \quad [G(\Delta x)]_j^n = u_{j+1}^n, \tag{A2}$$

$$\left[\frac{\partial}{\partial \Delta x} G(-\Delta x) \right]_j^n = \left(\frac{\partial u}{\partial x} \right)_{j-1}^n, \quad \text{and} \quad \left[\frac{\partial}{\partial \Delta x} G(\Delta x) \right]_j^n = \left(\frac{\partial u}{\partial x} \right)_{j+1}^n. \tag{A3}$$

Using relations (A2) and (A3), we can determine the high-order derivatives expressed by the displacement and its gradient. For convenience, we present the approximation formulas as follows

$$\partial_{2x} u_j^n = \frac{2}{\Delta x^2} \delta_x^2 u_j^n - \frac{1}{2\Delta x} \left(E_x^1 - E_x^{-1} \right) \partial_x u_j^n, \tag{A4}$$

$$\partial_{3x} u_j^n = \frac{15}{2\Delta x^3} \left(E_x^1 - E_x^{-1} \right) u_j^n - \frac{3}{2\Delta x^2} \left(E_x^1 + 8I + E_x^{-1} \right) \partial_x u_j^n, \tag{A5}$$

$$\partial_{4x} u_j^n = -\frac{12}{\Delta x^4} \delta_x^2 u_j^n + \frac{6}{\Delta x^3} \left(E_x^1 - E_x^{-1} \right) \partial_x u_j^n, \tag{A6}$$

$$\partial_{5x} u_j^n = -\frac{90}{\Delta x^5} \left(E_x^1 - E_x^{-1} \right) u_j^n + \frac{30}{\Delta x^4} \left(E_x^1 + 4I + E_x^{-1} \right) \partial_x u_j^n, \tag{A7}$$

where $\partial_{mx} u_j^n = \left(\partial^m u / \partial x^m \right)_j^n$, I is a unchangeable operator. δ_x^2 and E_x are the second central difference and displacement operators defined by

$$\delta_x^2 u_j^n = u_{j+1}^n - 2u_j^n + u_{j-1}^n,$$
$$E_x^1 u_j^n = u_{j+1}^n, \quad E_x^{-1} u_j^n = u_{j-1}^n.$$

Similarly, following the "analysis thought" (Konddoh *et al.*, 1994) and the original NADM (Yang *et al.*, 2003a), the approximation formulas for determining the high-order derivatives for the 2D acoustic case can be written as follows:

$$\partial_{2x} u_{i,j}^n = \frac{2}{\Delta x^2} \delta_x^2 u_{i,j}^n - \frac{1}{2\Delta x} \left(E_x^1 - E_x^{-1} \right) \partial_x u_{i,j}^n, \tag{A8}$$

$$\partial_{2z} u_{i,j}^n = \frac{2}{\Delta z^2} \delta_z^2 u_{i,j}^n - \frac{1}{2\Delta z} \left(E_z^1 - E_z^{-1} \right) \partial_z u_{i,j}^n, \tag{A9}$$

$$\partial_{3x} u_{i,j}^n = \frac{15}{2\Delta x^3} \left(E_x^1 - E_x^{-1} \right) u_{i,j}^n - \frac{3}{2\Delta x^2} \left(E_x^1 + 8I + E_x^{-1} \right) \partial_x u_{i,j}^n, \tag{A10}$$

$$\partial_{3z} u_{i,j}^n = \frac{15}{2\Delta z^3} \left(E_z^1 - E_z^{-1} \right) u_{i,j}^n - \frac{3}{2\Delta z^2} \left(E_z^1 + 8I + E_z^{-1} \right) \partial_z u_{i,j}^n, \tag{A11}$$

$$\partial_{2xz}u^n_{i,j} = \frac{1}{4\Delta x^2\Delta z}(5E^1_xE^1_z - 5E^{-1}_xE^{-1}_z + E^1_xE^{-1}_z - E^{-1}_xE^1_z - 4E^1_z + 4E^{-1}_z - 6E^1_x + 6E^{-1}_x)u^n_{i,j} + \frac{1}{2\Delta x\Delta z}(-E^1_xE^1_z - E^{-1}_xE^{-1}_z + E^1_x + E^{-1}_x - 2\delta^2_z)\partial_x u^n_{i,j} + \frac{1}{\Delta x^2}\delta^2_x(\partial_z u^n_{i,j}), \quad \text{(A12)}$$

$$\partial_{x2z}u^n_{i,j} = \frac{1}{4\Delta x\Delta z^2}(5E^1_xE^1_z - 5E^{-1}_xE^{-1}_z - E^1_xE^{-1}_z + E^{-1}_xE^1_z - 4E^1_x + 4E^{-1}_x - 6E^1_z + 6E^{-1}_z)u^n_{i,j} + \frac{1}{2\Delta x\Delta z}(-E^1_xE^1_z - E^{-1}_xE^{-1}_z + E^1_z + E^{-1}_z - 2\delta^2_x)\partial_z u^n_{i,j} + \frac{1}{\Delta z^2}\delta^2_z(\partial_x u^n_{i,j}), \quad \text{(A13)}$$

$$\partial_{4x}u^n_{i,j} = -\frac{12}{\Delta x^4}\delta^2_x u^n_{i,j} + \frac{6}{\Delta x^3}(E^1_x - E^{-1}_x)\partial_x u^n_{i,j}, \quad \text{(A14)}$$

$$\partial_{4z}u^n_{i,j} = -\frac{12}{\Delta z^4}\delta^2_z u^n_{i,j} + \frac{6}{\Delta z^3}(E^1_z - E^{-1}_z)\partial_z u^n_{i,j}, \quad \text{(A15)}$$

$$\partial_{2x2z}u^n_{i,j} = \frac{1}{\Delta x^2\Delta z^2}(E^1_xE^1_z + E^{-1}_xE^{-1}_z + E^{-1}_xE^1_z + E^1_xE^{-1}_z - 2\delta^2_x - 2E^1_z - 2E^{-1}_z)u^n_{i,j}, \quad \text{(A16)}$$

$$\partial_{5x}u^n_{i,j} = -\frac{90}{\Delta x^5}(E^1_x - E^{-1}_x)u^n_{i,j} + \frac{30}{\Delta x^4}(E^1_x + 4I + E^{-1}_x)\partial_x u^n_{i,j}, \quad \text{(A17)}$$

$$\partial_{5z}u^n_{i,j} = -\frac{90}{\Delta z^5}(E^1_z - E^{-1}_z)u^n_{i,j} + \frac{30}{\Delta z^4}(E^1_z + 4I + E^{-1}_z)\partial_z u^n_{i,j}, \quad \text{(A18)}$$

$$\partial_{4xz}u^n_{i,j} = \frac{-3}{\Delta x^4\Delta z}(5E^1_xE^1_z - 5E^{-1}_xE^{-1}_z + E^1_xE^{-1}_z - E^{-1}_xE^1_z - 4E^1_z + 4E^{-1}_z - 6E^1_x + 6E^{-1}_x)u^n_{i,j} + \frac{6}{\Delta x^3\Delta z}(E^1_xE^1_z + E^{-1}_xE^{-1}_z + 2\delta^2_z - E^1_x - E^{-1}_x)\partial_x u^n_{i,j}, \quad \text{(A19)}$$

$$\partial_{x4z}u^n_{i,j} = \frac{-3}{\Delta x\Delta z^4}(5E^1_xE^1_z - 5E^{-1}_xE^{-1}_z - E^1_xE^{-1}_z + E^{-1}_xE^1_z - 4E^1_x + 4E^{-1}_x - 6E^1_z + 6E^{-1}_z)u^n_{i,j} + \frac{6}{\Delta x\Delta z^3}(E^1_xE^1_z + E^{-1}_xE^{-1}_z + 2\delta^2_x - E^1_z - E^{-1}_z)\partial_z u^n_{i,j}, \quad \text{(A20)}$$

$$\partial_{3x2z}u^n_{i,j} = \frac{3}{\Delta x^3\Delta z^2}(E^1_xE^1_z - E^{-1}_xE^{-1}_z + E^1_xE^{-1}_z - E^{-1}_xE^1_z - 2E^1_x + 2E^{-1}_x)u^n_{i,j} - \frac{6}{\Delta x^2\Delta z^2}\delta^2_z(\partial_x u^n_{i,j}), \quad \text{(A21)}$$

$$\partial_{2x3z}u^n_{i,j} = \frac{3}{\Delta x^2\Delta z^3}(E^1_xE^1_z - E^{-1}_xE^{-1}_z + E^{-1}_xE^1_z - E^1_xE^{-1}_z - 2E^1_z + 2E^{-1}_z)u^n_{i,j} - \frac{6}{\Delta x^2\Delta z^2}\delta^2_x(\partial_z u^n_{i,j}), \quad \text{(A22)}$$

where $\partial_{mxkz}u^n_{i,j} = (\partial^{m+k}u/\partial x^m\partial z^k)^n_{i,j}$, $\partial_{mxz}u^n_{i,j} = (\partial^{m+1}u/\partial x^m\partial z)^n_{i,j}$, $\partial_{xmz}u^n_{i,j} = (\partial^{m+1}u/\partial x\partial z^m)^n_{i,j}$, and these notations in equations (A8) to (A22) denote the same significance as those presented in equations (A4) to (A7). For example, δ^2_z and E_z are the second central difference and displacement operators in the z direction, which are defined by

$$\delta^2_z u^n_{i,j} = u^n_{i,j+1} - 2u^n_{i,j} + u^n_{i,j-1},$$
$$E^1_z u^n_{i,j} = u^n_{i,j+1}, \quad \text{and } E^{-1}_z u^n_{i,j} = u^n_{i,j-1}.$$

Appendix B

Derivation of Stability Criteria

1D Homogeneous Case

To obtain the stability conditions, we consider harmonic solutions of equation (6). Substituting the solution

$$U_j^n = \begin{pmatrix} u \\ v \end{pmatrix}^n \exp(i(kjh)), \tag{B1}$$

into equation (6) with relations (A4) to (A7), we can obtain the following equation

$$(u^{n+1}, \tilde{u}^{n+1}, v^{n+1}, \tilde{v}^{n+1})^T = A(u^n, \tilde{u}^n, v^n, \tilde{v}^n)^T, \tag{B2}$$

where k is the wavenumber, $v = \partial u/\partial x$, $\tilde{u}^n = u^{n-1}$, $\tilde{v}^n = v^{n-1}$, and the matrix A is

$$A = \begin{bmatrix} 2-2a_1 & -ib_1 & -1 & 0 \\ ia_2 & 2-2b_2 & 0 & -1 \\ 1 & 0 & 0 & 0 \\ 0 & 1 & 0 & 0 \end{bmatrix} \tag{B3}$$

with

$$a_1 = \alpha^2(-2 + \alpha^2)(\cos(kh) - 1),$$

$$a_2 = 15\alpha^2(1 - \alpha^2)\sin(kh)/h,$$

$$b_1 = c_0\Delta t\alpha(1 - \alpha^2)\sin(kh),$$

$$b_2 = \alpha^2[3(\cos(\mathrm{kh}) + 4) - 5\alpha^2(\cos(kh) + 2)],$$

in which the Courant number (Dablain, 1986; Sei and Symes, 1994) is defined by $\alpha = c_0\,\Delta t/h$ with $h = \Delta x$.

From the matrix A we can obtain numerically the following stability condition via solving the eigenvalues of satisfying $|\lambda(A)| \le 1$ of the matrix A:

$$\alpha \le \alpha_{\max} \approx 0.754, \tag{B4}$$

or

$$\Delta t \le \alpha_{\max}\frac{h}{c_0} \approx 0.754\,\frac{h}{c_0},$$

where $\alpha_{\max}$ denotes the maximum Courant number that keeps the numerical calculation stable.

2D Homogeneous Case

For the 2D problem, we consider the case of $\Delta x = \Delta z = h$. In the case we are considering the derivation follows the same steps as in the 1D case and we can obtain the stability condition for the 2D case similarly is follows:

$$\alpha \le \alpha_{\max} \approx 0.527, \tag{B5}$$

or

$$\Delta t \le \alpha_{\max}\frac{h}{c_0} \approx 0.527\,\frac{h}{c_0}.$$

Appendix C

Derivation of the Dispersion Relation

To minimize the dispersion error, we derive the dispersion relation of the ONADM. For this, following the analysis methods presented in Dablain, (1986) and Wang *et al.* (2002), we consider the harmonic solution of equation (6) and substitute the solution

$$U_j^n = \begin{pmatrix} u_0 \\ v_0 \end{pmatrix} \exp[i(\omega_{\mathrm{num}} n\Delta t + kjh)], \tag{C1}$$

into equations (6) and (A4) to (A7) to obtain the following dispersion equation:

$$4(\cos\gamma - 1)^2 + 2(a + b)(\cos\gamma - 1) + ab - d\sin^2\theta = 0, \tag{C2}$$

where

$$\gamma = \omega_{\mathrm{num}}\,\Delta t, \quad \theta = kh,$$

$$a = \alpha^2(1 - \cos\theta)(4 - 2\alpha^2),$$

$$b = \alpha^2[3(4 + \cos\theta) - 5(2 + \cos\theta)\alpha^2],$$

$$d = 15\alpha^4(1 - \alpha^2)^2.$$

Using the dispersion relation (C2), we obtain the ratio of the numerical velocity to the phase velocity c_0 as follows:

$$R_{\mathrm{ONADM}} = \frac{c_{\mathrm{num}}}{c_0} = \frac{\gamma}{\alpha\theta}, \tag{C3}$$

where γ satisfies the dispersion equation (C2).

For comparison, here we also present the dispersion relation of Dablain's high-order compact schemes (Dablain, 1986). On the basis of the Lax–Wendroff scheme, Dablain (1986) developed the high-order compact methods with different accuracies as follows:

$$\left(\frac{\partial^2 u}{\partial x^2}\right)_j^n = \frac{1}{\Delta x^2}\left[w_0 u_j^n + \sum_{i=1}^{M} w_i(u_{j+i}^n + u_{j-i}^n)\right], \tag{C4}$$

Table C1
The Coefficients of the LWC with Different Accuracies (Dablain, 1986)

Methods	w_0	w_1	w_2	w_3	w_4	w_5
$O(\Delta t^4, \Delta x^4)$	−5/2	4/3	−1/12			
$O(\Delta t^4, \Delta x^6)$	−49/18	3/2	−3/20	1/90		
$O(\Delta t^4, \Delta x^8)$	−205/72	8/5	−1/5	8/315	−1/560	
$O(\Delta t^4, \Delta x^{10})$	−2.927222	1.666667	−0.238095	0.039683	−0.004960	0.000317

where $M = 2, 3, 4$, and 5 denote the methods with accuracies of $O(\Delta t^4, \Delta x^4)$, $O(\Delta t^4, \Delta x^6)$, $O(\Delta t^4, \Delta x^8)$, and $O(\Delta t^4, \Delta x^{10})$, respectively. These coefficients in equation (C4) are presented in Table C1. Equation (C4) shows that Dablain's LWC or high-order compact scheme uses 5, 7, 9, and 11 grid points in a direction for the fourth-, sixth-, eighth-, and tenth-order LWCs, respectively, whereas the ONADM only uses three grid points seen from equations (A4) (A5), (A6), (A7) presented in Appendix A.

Similarly, we can obtain the ratio of the numerical velocity to the phase velocity for the high-order compact schemes with different accuracies as follows:

$$R_{L-W} = \frac{c_{\text{num}}}{c_0} = \frac{\arccos(1 + e/2)}{\alpha\theta}, \tag{C5}$$

where

$$e = \alpha^2 b + \frac{1}{6}\alpha^4\Big[- b + w_0 \cos\theta + \sum_{i=1}^{M} w_i[\cos(i+1)\theta + \cos(i-1)\theta]\Big], \tag{C6}$$

$$b = w_0 + 2\sum_{i=1}^{M} w_i \cos(i\theta). \tag{C7}$$

Appendix D

Derivation of Theoretical Errors

1D Case

We rewrite equation (1) as follows

$$(D_{2t} - D_{2x})u = 0, \tag{D1}$$

where: $D_{2t} = \partial^2/\partial t^2$ and $D_{2x} = c_0^2\partial^2/\partial x^2$ are the exact derivative operators with respect to time and space.

We can define the following ONADM temporal operator, derived from equation (6) and used equations (1) and (A4):

$$L_{2t}u_j^n = \frac{1}{\Delta t^2}\left[\delta_t^2 u_j^n - \frac{(c_0\Delta t)^4}{12}\partial_{4x}u_j^n\right], \tag{D2}$$

and the ONADM spatial operator

$$L_{2x}u_j^n = \frac{2}{\Delta x^2}\delta_x^2 u_j^n - \frac{1}{2\Delta x}(E_x^1 - E_x^{-1})\partial_x u_j^n. \tag{D3}$$

Then the first equation of the vector equation (6) can be written as follows:

$$(L_{2t} - c_0^2 L_{2x})u_j^n = 0. \tag{D4}$$

The operator error of the ONADM is computed by a Taylor series expansion. Omitting details, we obtain the following errors of temporal and spatial operators:

$$(D_{2t} - L_{2t})u_j^n = -\frac{\Delta t^4}{360}\partial_{6t}u_j^n + O(\Delta t^6), \tag{D5}$$

$$(D_{2x} - c_0^2 L_{2x})u_j^n = \frac{c_0^2\Delta x^4}{360}\partial_{6x}u_j^n + O(\Delta x^6). \tag{D6}$$

Using equation (1) and combining the preceding results, we obtain the theoretical error E_1 of the ONDAM operator:

$$\begin{aligned} E_1 &= [(D_{2t} - L_{2t}) - (D_{2x} - c_0^2 L_{2x})]u_j^n \\ &= -c_0^2\frac{(\alpha^4 + 1)\Delta x^4}{360}\partial_{6x}u_j^n + O(\Delta x^6 + \Delta t^6). \end{aligned} \tag{D7}$$

In the ONADM algorithm we must solve the gradient of the displacement u at each timestep. To keep the ONADM calculation stable, we should also give the stable condition of computing the gradient of the displacement.

Obviously, the gradient of the displacement u for the homogeneous case satisfies the following equation:

$$\frac{\partial^2}{\partial t^2}\left(\frac{\partial u}{\partial x}\right) = c_0^2\frac{\partial^3 u}{\partial x^3}. \tag{D8}$$

When we use the ONADM to solve equation (D8) to obtain the gradient of the displacement, we similarly have the following theoretical error E_2 of the ONDAM operator:

$$E_2 = [(D_{2t} - L_{2t}) - (D_{2x} - c_0^2 L_{2x})]\partial_x u_j^n = -c_0^2 \frac{(7\alpha^4 + 3)\Delta x^4}{2520} \partial_{7x} u_j^n + O(\Delta x^6 + \Delta t^6). \quad \text{(D9)}$$

2D Case

For the 2D case, we consider the case of $\Delta x = \Delta z = h$. In the case we are considering the derivation follows the same steps as in the 1D case and we can similarly obtain the following theoretical error E_1 of the ONDAM operator for solving equation (2):

$$E_1 = -\frac{c_0^2 h^4}{360} [(1+\alpha^4)(\partial_{6x} + \partial_{6z}) + 3\alpha^4(\partial_{4x2z} + \partial_{2x4z})]u_{i,j}^n + O(\Delta t^6 + h^6) = O(\Delta t^6 + h^4). \quad \text{(D10)}$$

From equation (2) the gradient of the displacement u yields the following equations:

$$\frac{\partial^2}{\partial t^2}\left(\frac{\partial u}{\partial x}\right) = c_0^2\left(\frac{\partial^3 u}{\partial x^3} + \frac{\partial^3 u}{\partial x \partial z^2}\right), \text{ and} \quad \text{(D11)}$$

$$\frac{\partial^2}{\partial t^2}\left(\frac{\partial u}{\partial z}\right) = c_0^2\left(\frac{\partial^3 u}{\partial x^2 \partial z} + \frac{\partial^3 u}{\partial z^3}\right). \quad \text{(D12)}$$

When using the ONADM to solve equations (D11) and (D12) to obtain the first derivative of the displacement u with respect to x and z, we use a procedure deduced similarly, to that stated previously to obtain the theoretical errors of the ONADM. These errors are

$$E_2 = O(\Delta t^6 + h^4), \quad \text{(D13)}$$

$$E_3 = O(\Delta t^6 + h^4). \quad \text{(D14)}$$

Department of Mathematical Sciences
Tsinghua University
Beijing 100084, People's Republic of China
dhyang@math.tsinghua.edu.cn
(D.Y., M.L.)

Department of Computing and Software
McMaster University
Hamilton, Ontario, Canada L8S 4L7
pengi@mcmster.ca
terlaky@mcmaster.ca
(J.P., T.T.)

Manuscript received 15 April 2005.